Volume 12 (Issue.12),
October, 2021

ISSN-2230-9578

Journal of Research and Development

- A Multidisciplinary International Level Reviewed Journal

COSMOS
IMPACT FACTOR
7:26

Editor
Dr. R. V. Bhole

'Ravichandram' Survey No-101/1, Plot No-23, Mundada Nagar, Jalgaon (M.S.) 425102
Email- rbhole1965@gmail.com Visit-www.jrdrvb.com

ISSN-2230-9578

Journal of Research and Development

Volume 12 (Issue 12) October, 2021

सम्पादक –

प्रा. डॉ. आर. व्ही. भोळे

संपादकीय कार्यालय

Journal of Research and Development
C/o Dr. V. J. Patil, 'Prajyot', Plot No. 8, Survey No. 101/2, Mundada Nagar, Jalgaon (M.S.) 425002

१) सम्पादन – प्रकाशन एवं संचालन अवैतनिक

२) कला साहित्य संस्कृती समाज इतिहास राजनिती एवं आर्थिक विषयों पर केंद्रीत शोधपत्र आमंत्रित है।

३) जर्नल ऑफ रिसर्च ॲन्ड डेव्हलपमेंट में प्रकाशित शोध/विचार पत्रों में व्यक्त चिन्तन एवं दृष्टीकोन सम्बधित लेखकों के है। उससें जर्नल का सहमत होना आवश्यक नही है।

४) सदस्यता फार्म एवं नियमावली अंक के अंतिम पृष्ट पर देखे।

५) जर्नल ऑफ रिसर्च ॲन्ड डेव्हलपमेंट का प्रकाशन प्राध्यापकों को प्राध्यापकों के द्वारा, प्राध्यापकों के लिए एक अव्यावसायिक सहयोगी प्रयास।

६) सदस्यता शुल्क का भुगतान नगद मनी ऑर्डर व्दारा जर्नल ऑफ रिसर्च ॲन्ड डेव्हलपमेंट जलगांव के पतेपर भिजवाए।

७) मराठी भाषाके शोध पत्र प्रकाशित किए जाएगे।

८) इस शोध पत्रिका को प्रकाशित करते हुए पुर्ण सावधानी बरती गई है। फिर भी किसी प्रकारकी त्रृटि के लिए सम्पादक प्रकाशक मुद्रक जिम्मेदार नही होगा। समस्त विवादों का न्यायक्षेत्र जळगांव होगा।

९) जर्नल ऑफ रिसर्च ॲन्ड डेव्हलपमेंट में प्रकाशनार्थ प्राप्त होने वाले शोधपत्रो का चयन एव उनकी स्वीकृती । अस्वीकृती का निर्णय सम्पादन मंडल द्वारा लिया जाता है।

ISSN-2230-9578

Journal of Research and Development
Volume 12 (Issue 12) October, 2021

INDEX

Journal of Research & Development
Vol. 12 (Issue 12), October, 2021
(ISSN-2230-9578)

Supercapacitive properties of hybrid PANI-$Ni(OH)_2$ nanocomposite electrodes

Janardhan H. Shendkar
S. S. J. E. S. Arts, Commerce & Science College, Gangakhed, Dist. Parbhani, India

Abstract
Nanocomposite (NC) hybrid electrodes of polyaniline (PANI)-nickel hydroxide [$Ni(OH)_2$] have been prepared by two-step electrodeposition processes onto stainless-steel (SS) substrates. Enhanced stability of amorphous PANI- $Ni(OH)_2$ NC electrodes with loading of $Ni(OH)_2$ electrode materials have been explored. PANI has a nanofibrous morphology and on account of less loading of $Ni(OH)_2$, the NC electrodes retain an overall nanofibrous morphology. The maximum specific capacitance (SC), obtained from integrated charge under voltammetric conditions, for NC (electrodeposition of $Ni(OH)_2$ for 05 min and 15 min onto PANI electrode surface) electrodes, are 20.08 F/g & 33.48 F/g, respectively. The retention in SC values with scan rates from 10 to 100 mV/s for NC (05 min) and NC (15 min) are 66.6% & 37.3% respectively. The retention in SC values with increase of cycle number up to 1000 for NC (05 min) and NC (15 min) electrodes are 56.6% and 59.35% respectively, demonstrating higher electrochemical stability of NC electrodes with loading time of $Ni(OH)_2$. Nearly 22.5 and 37.5 mC/cm2 charges, NC (05 min) and NC (15 min) electrodes are obtained respectively.

Keywords
Electrochemical Supercapacitors, Nanocomposite, Polyaniline, Specific capacitance, nanostructures, Nickel hydroxide, electrodeposition

1 Introduction

Electrochemical supercapacitors (ES) have captivated appreciable attention in recent years, as they are competent to provide high power density, long cyclability and fast charge/discharge capability [1]. Their use in consumer electronics like memory back-up systems, digital communications, electrical vehicles and industrial power/energy management etc., is widely known [2]. Based on their charge storage mechanism they are of two categories i.e. electrical double layer capacitor and pseudocapacitor or faradaic capacitor. In an electric double layer capacitor energy is physically stored by means of ion adsorption at the electrode/electrolyte interface to form electric double layer whereas in pseudocapacitor energy is stored chemically due to reversible surface or near-surface faradaic reactions. As a result, the specific capacitance (SC) of the ES is proportional to the accessible surface area of the electrode materials to the electrolyte ions for redox reactions/electric double layer formation. In the preparation of SCs, the material of electrode is one of the key factors affecting the performance of ECs. Therefore, the SC

value of active material can be increased by converting the bulk structure electrode material to the nanostructure materials to provided high surface area on account of extremely small in particle size and refined nano-morphological structure, which shortens the path length of ion transfer to release mechanical stress during charge/discharge process [1, 3-8]. Polyaniline (PANI) is one of the conducting polymer material used for ES due to availability of several preparative methods for distinguishable morphologies, inexpensive with environmental and chemical stabilities etc. [9]. Out of all morphologies nanofibers/ nanowires have attracted more attention due to their low inter-particle contact resistance; higher conductivity and high accessible surface area have provided high SC value [10]. The backbone of PANI contains alternating nitrogen atoms and benzene rings. PANI exists in form of base and/or salt in three isolable oxidation states; leucoemeraldine (fully reduced form with pale yellow colour), emeraldine (half-oxidized and protonated form with green colour or half oxidized form with blue colour), and pernigraniline (fully oxidized form with blue/violet colour) depending upon the degree of oxidation of the nitrogen atoms. Of these, only emeraldine salt is electrically conductive [11] due to possibility of supporting polaron or bipolarons as charge carriers. The main drawback of PANI electrode lies not only in its lower cycle stability but also in electrochemical inactivity in alkaline solution [12]. Hence, it is essential to make composite of the PANI with another suitable supercapacitive electrode material to produce nanostructure morphology to not only overcome the stability but also to achieve the novel properties of the nanocomposite (NC) electrode useful for supercapacitive properties. NCs of PANI with polymer [13], metals [14], metal oxides [15], carbon [16] and graphite [17] have been studied and achieved the goals of high capacitance and better stability.

Among the series of the transition metal oxides/hydroxides, nickel hydroxide [$Ni(OH)_2$] is one of the electro-active metal hydroxides used as ES material. Due to well defined redox activity, high theoretical supercapacitive value, low-cost and layered morphology, nickel hydroxide becomes one of the important supercapacitive electrode material and hence from decade this material is at the centre of research [18, 19]. However, it suffers from drawback of weak adhesion between the nickel-based material and the current collector (substrate), leading to the loss of active material, which shortens cycle life as a supercapacitor electrode [20]. In order to overcome this drawback, NCs of $Ni(OH)_2$ with MnO_2 [21], Ni_3S_2/3DGN (three dimensional graphene network)[22], graphene oxide [23], CoO/rGO [24], Co_3O_4/RGO [25] etc., have been with positive results.

In the preset work, PANI/$Ni(OH)_2$ NC electrodes were developed by using electrodeposition method and their structural, elemental analysis, morphological and electrochemical properties like CV, galvanostatic charge-discharge and electrochemical impedance are studied and explored. The electrodeposition of $Ni(OH)_2$ onto the PANI electrode has been carried out at negative potential, hence both process of reduction of PANI and electrodeposition of $Ni(OH)_2$.

2 Experimental section

2.1 Materials

Aniline, nickel nitrate hexahydrate, sulphuric acid, acetone and sodium hydroxide of analytical reagent grade were purchased from Merck. The distilled water and all reagents were used without further purification.

2.2 Preparation of PANI-$Ni(OH)_2$ NC electrode

Polymerizations of aqueous 0.5M aniline and 0.5M sulphuric acid solution into PANI were carried out at constant potential of 0.75V for 5 minutes in a standard three-electrodes glass cell; consisting of stainless-steel (SS) of 1cm x 4cm as working electrode, a platinum plate of 1.5cm x 1.5cm, as counter electrode and Ag/AgCl electrode as reference electrode. The working electrodes were cleaned with first by acetone and then by distilled water ultrasonically; after polishing with emery paper, and dried in an air before each trial. The depth and distance of the working electrode in a solution was kept 1cm from solution surface as well as from the reference and counter electrode. The PANI electrodes were electrodeposited on one side of SS substrate ($1cm^2$) which was dried in air before and after immersion in distilled water for 2 min for further use.

Electrodeposition of PANI-$Ni(OH)_2$ NC electrodes were obtained using aqueous solution of 0.05M nickel nitrate hexahydrated at a constant potential of -1.0V for 5minutes (A) and 15minutes (B) onto PANI electrode. As prepared NC electrodes were immersed in distilled water for 2 min and dried in air at room temperature before next characterizations.

2.3 Characterization techniques

X-ray diffraction (XRD) measurements were carried out by using a (Ultima IV, Rigaku 2500) diffractometer with a Cu"Ká radiation in the 2è range of 10"80°. The morphologies and elemental analysis of the electrodes material were investigated on field-emission scanning electron microscope (FE-SEM), Hitachi S-4800. The electrochemical deposition and the CV of the NC film electrodes were carried out through a WonAtech (WPG 100 Potentiostat / Galvanostat) electrochemical workstation. The electrochemical impedance spectroscopy (EIS) studies were performed on IVIUM STAT workstation, The Netherlands. All the electrochemical properties were studied in 1.0M NaOH electrolyte solution.

3 Results and Discussion

3.1 Reaction kinetics

The electrodeposition of aqueous solution of aniline + sulphuric acid resulted in green coloured PANI electrode at a constant potential of +0.75V. According experimental conditions, under applied constant potential in three electrodes system, a current through the conducting substrate causes initially to deposit a compact layer/film of PANI, which means the rate of lateral electrodeposition along surface of substrate, was initially greater than vertical deposition. Then the growth of PANI takes place along one dimension i.e. vertical to the surface of substrate, as the aniline monomer being continuously consumed

in the deposition process instead of forming new nuclei. The further process of electrodeposition resulted in the elongation of length along the initially deposited nuclei to form the nanofiber/nanowire type morphology of PANI [26]. The electrodeposition of $Ni(OH)_2$ from the $Ni(NO_3)_2$ precursor was due to a reduction of the nitrate ions on the PANI-SS electrode surface to produce hydroxide ions [27]. There is a raise of local pH on account of the generation of the OH> ions, resulting in reaction between nickel ion and hydroxide ion in the form of the precipitation of $Ni(OH)_2$ at the electrode surface as by reactions;

$$NO_3^- + 7H_2O + 8e^- \rightarrow NH_4^+ + 10\ OH^- \quad (1)$$

$$Ni^{2+} + 2\ OH^- \rightarrow Ni(OH)_2 \quad (2)$$

In $Ni(OH)_2$ electrodeposition, the concentration of the $Ni(NO_3)_2$ precursor (0.05M) was low in order to make 100% utilization of electrochemically generated OH^- ions because at high concentration, $Ni_4(OH)_4^{4+}$ is formed at electrode surface which diffuses away OH^- ions from the reaction interface before deposition occurs [28, 29]. At the time of electrodeposition of the $Ni(OH)_2$ onto the PANI, PANI undergoes reduction from emeraldine state to leucoemeraldine state with time, as its colour was changed from green to greenish yellow or pale yellow.

3.2 Structural Elucidation

Fig. 1 shows the XRD patterns of the PANI/ $Ni(OH)_2$ NC electrodes. The same nature of intensity peaks in all XRD patterns marked * allow us to conclude as the peaks are of SS substrate. As all peaks are resemble to peaks of SS and there was no trace peak of either PANI or $Ni(OH)_2$, confirming an amorphous nature of both NCs. But in present study PANI gets reduced at the time of electrodeposition of $Ni(OH)_2$ into leucoemeraldine state having amorphous nature and the less availability of time for the arrangement of Ni^{2+} ions with respect to OH^- ions produce amorphous structure of NCs (A) & (B) electrodes.

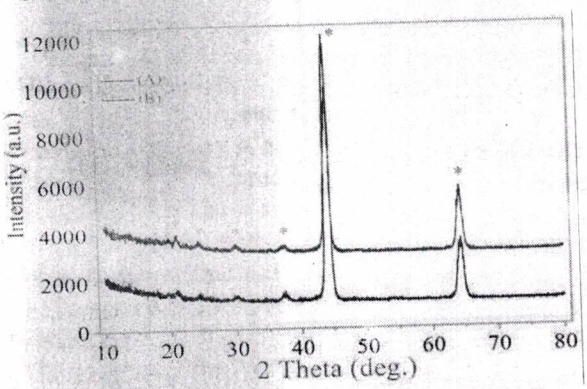

Fig. 1 XRD patterns of NCs (A) and (B) electrodes.

3.3 Surface Morphology

The FESEM images of the NC (A) and (B) electrodes are presented in Fig. 2. The FESEM of PANI electrode surface confirms nanofiber-type morphology. The nanofibers of PANI were non-uniform in sizes and shapes. These nanofibers were not grown in a straight line but bend to form secondary growth. The SEM images of the NCs of PANI and $Ni(OH)_2$ shows no much more changes in the nanofiber morphology, as deposition of $Ni(OH)_2$ on PANI is relatively very low due to two reasons, i) the reduction of the emeraldine state of PANI into leucoemeraldine state of PANI, so some part of potential/current utilized in reduction of PANI and remaining part of voltage/current utilized in reduction of nitrate ions; ii) the leucoemeraldine state of PANI is an electrically non-conducting, but for this conversion it takes some time at which the $Ni(OH)_2$ deposited in porous PANI nanofiber, which is an insufficient loading of $Ni(OH)_2$ mass on PANI nanofiber to form platelet/ nanofiber composite morphology (as can seen from EDX spectrum Fig. 3).

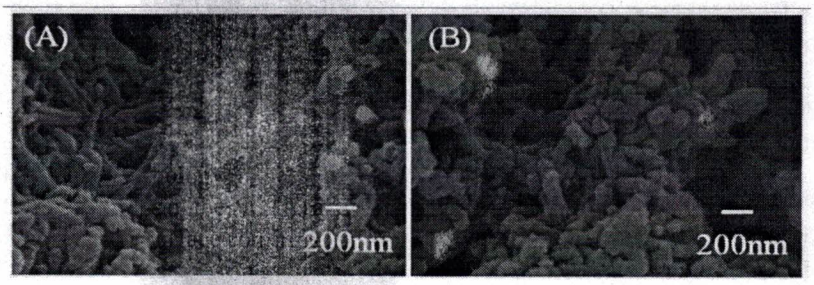

Fig. 2 FESEM images of NC (A) and (B) electrode surfaces.

3.4 Chemical composition analysis

Fig. 3 shows energy dispersive X-ray analysis (EDX) spectra of NCs (A) and (B) electrodes. These emitted characteristic x-ray spectral peaks qualitatively gives the information of presence of *C, N, Ni* and *O* in both NCs for PANI and $Ni(OH)_2$ indicates the formation of NCs. The spectral peak at about 2.15 keV in all EDX spectra may be the existence of spectral artifacts such as escape peak.

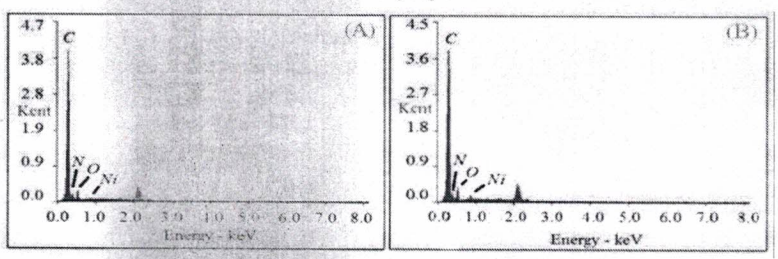

Fig. 3 EDX of NCs (A) and (B) electrodes.

3.5 Electrochemical measurements

3.5.1 CVs and electro-active measurements

The capacitive behaviour of electrode materials are generally characterized using CV curves. Fig. 4 presents typical CV curves of the (A) and (B) electrodes in 1.0M NaOH electrolyte at a scan rate of 10mV/s, in the potential range from 0.1V to 0.5V. In these CV curves, one pair of redox peak for Faradaic redox reactions are seen, suggesting the capacitance is mainly due to Faradaic redox reactions. The anodic current in CV of NCs has greater value than cathodic current. The current in CV increased with potential window voltage to reach the maximum value due to redox reaction of active species of electrodes and then decreased due to unavailability of active species for redox reaction with increase in potential window voltage, indicates towards the variation of ohmic drop across the electrode material during CV. Therefore, the current before starting redox reaction and after completion of redox reaction may be due to electrolyte ion deposition to form electric double layer. Thus, the capacitance of NC electrodes in alkaline electrolyte solution is from the charge storage in the electric double layer at the electrode/electrolyte interface and charge storage in the electrode material by redox reactions on the surface and hydroxyl ion diffusion in the electrode active material [30]. For the $Ni(OH)_2$, in alkaline medium, the surface Faradaic reaction follows [31]

$$Ni(OH)_2 + OH > \text{"! } NiOOH + H_2O + e> \qquad (3)$$

From the observations of CV curves, it can be inferred that, the capacitance is majorly from the $Ni(OH)_2$ rather than PANI in NC electrodes as much more capacitance is stored in a redox capacitor than in a double-layer capacitor. Area of CV curve, the charge density, specific capacitance, energy density and power density values of the electrodeposited individual and NC electrodes were calculated from the CV curves, according to the following equation

$$A = \int I(V)dV \qquad (4)$$

$$q = \frac{1}{v}\int I(V)dV \qquad (5)$$

$$C_s = \frac{q}{m\nabla V} \qquad (6)$$

$$E = \frac{1}{2}C_s(\nabla V)^2 \qquad (7)$$

$$P = \frac{1}{2}C_s(\nabla V)\frac{dV}{dt} \qquad (8)$$

where, A is area of the closed CV curve (mW), q is the charge density (mC/cm^2), $v = dV/dt$ is scan rate (mV/s), Cs is specific capacitance (F/g), m is mass of electrode materials (g), ∇V is the potential window of CV, E is energy density (Wh/kg) and P is power density (W/kg).

The SC values calculated at scan rate of 10mV/s for (A) and (B) electrodes were 20.08 F/g & 33.48 F/g respectively. In the present case, with electrodeposition time of $Ni(OH)_2$ onto PANI electrode, the SC values are maintained in NCs.

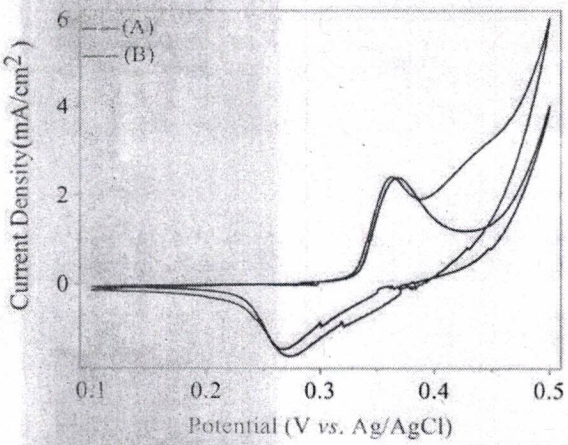

Fig.4 CV curves of NC- (A) and (B) electrodes in 1.0 M NaOH electrolyte.

3.5.2 Scan Rate Effect

The CV curve for relationship between current densities and scan rates has been investigated for both electrodes at scan rate from 10mV/s to 100mV/s are shown in Fig. 5. The shape of anodic and cathodic CV curve remained same for both electrodes. With increasing the scan rate, the current density and hence peak current density of CV also increased and the oxidation peaks shifted to a more positive position and the reduction peaks slightly to a more negative position due to an increase of the internal diffusion resistance within the electro-active material with an increase in scan rate [32]. The increase in current density with scan rate was not linear, suggesting the assessable active sites of electrode material by electrolyte species (cations /anions) were diffusion limited than surface limited as the diffusion of electrolyte ions decreases with increasing scan rate, which does not maintain the peak current density with scan rate. The dependence of A, q, Cs, E and P with scan rate are depicted in Table 1. The retention in q, Cs and E is same and is 66.6% & 37.3% respectively for electrodes (A) and (B). Therefore, electrode (A) has maximum retention than (B) electrodes, with an increase in scan rate from 10 to 100mV/s, suggesting much better rate capability in NC electrode (A) as well as good ion diffusion and electron transport ability at high current density. The retention in area of CV curve and P is same and is 85.0%, and 73.2% respectively for electrodes (A) and (B). In this case we find that the energy density for both electrodes decreased with increase in power density with increase in scan rate.

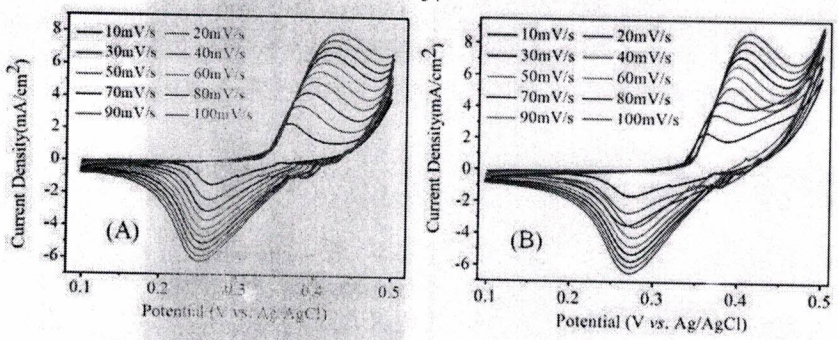

Fig.5 Scan rate effect CV curves for electrodes (A) and (B).

Table1 Numerical values of A, q, Cs, E and P with scan rate for electrodes (A) and (B).

Scan Rate/ Electr -odes	Physical Quantities	10	20	30	40	50	60	70	80	90	100	% of Reten-tion
(A)	A (mW)	0.225	0.45	0.6	0.75	0.95	1.05	1.15	1.3	1.4	1.5	85%
	q (mC/cm²)	22.5	22.5	20.0	18.75	19.0	17.5	16.42	16.25	15.55	15.0	66.6%
	Cs (F/g)	20.08	20.08	17.85	16.74	16.96	15.62	14.66	14.50	13.88	13.39	
	E (Wh/kg)	0.446	0.446	0.396	0.372	0.376	0.347	0.325	0.322	0.308	0.297	
	P (W/kg)	40.17	80.35	107.1	134.0	169.6	187.5	205.3	232.1	249.9	267.8	85%
(B)	A (mW)	0.375	0.60	0.75	0.8	0.92	1.0	1.1	1.25	1.35	1.4	73.2%
	q (mC/cm²)	37.5	30.0	25.0	20.0	18.4	16.66	15.71	15.62	15.0	14.0	37.3%
	Cs (F/g)	33.48	26.78	22.32	17.85	16.42	14.88	14.03	13.65	13.39	12.5	
	E (Wh/kg)	0.744	0.595	0496	0.396	0.365	0.330	0.311	0.310	0.297	0.277	
	P (W/kg)	66.96	107.7	133.9	142.8	164.2	178.5	196.4	223.2	241.0	250.0	73.2%

3.5.4 Cyclic Stability

As, for real supercapacitor operations and applications, besides high specific capacitance, an excellent long cycle life stability is also required. Therefore, cyclic stability test with CV curves at a scan rate of 40mV/s with a potential range from 0.1V to 0.5V for electrodes (A & B), was carried out and given in Fig. 6 for 1000 cycles. The variation of q, Cs, E and P demonstrated a same nature of decrease in the values of electrodes (A) and (B) with a retention of 56.6% and 59.35% respectively as in Table 2, indicating an improvement in the cyclic stability of NC electrodes with time of electrodeposition. The CV curves of NC electrodes demonstrated well-defined pair of oxidation/reduction peaks from 1 to 1000 cycles. In the stability CV curves of electrodes (A) & (B), the oxidation and reduction peak potentials were shifted towards more positive potential. The differences of oxidation and reduction peak potentials of electrodes (A) and (B) for 1 to

1000 cycles were 0.154 to 0.153V and 0.136 to 0.132V, respectively. The potential difference between the oxidation potential and the reduction potential is a measure of the reversibility of the redox reaction and the relatively small values obtained here was an indication of a better reversibility [33-35] in NC electrode which is also evidenced from Table 2.

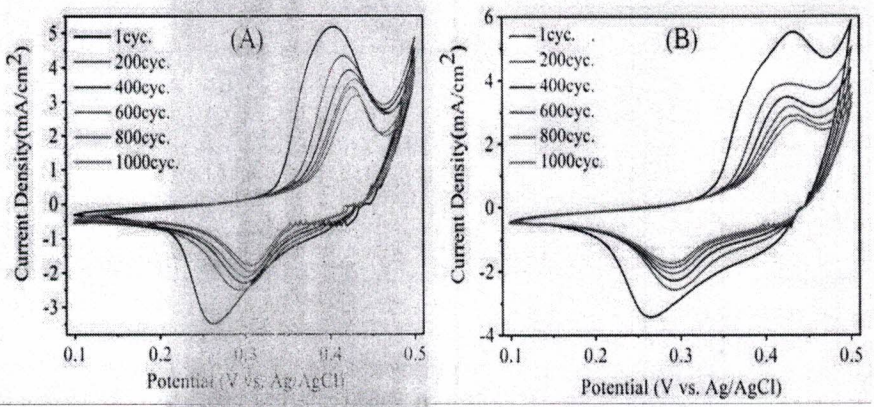

Fig. 6 Stability CV curves of (A) and (B) electrodes.

Table 2, Numerical values of A, q, Cs, E and P and cycle number for electrodes (A) & (B).

Cycle NO. /Electrodes	Physical Quantities	1	200	400	600	800	1000	% of Retention
(A)	A (mW)	0.75	0.675	0.575	0.5	0.425	0.425	56.60%
	q (mC/cm²)	18.75	16.87	14.37	12.5	10.62	10.62	
	Cs (F/g)	16.74	15.06	12.83	11.16	9.48	9.48	
	E (Wh/kg)	0.372	0.334	0.285	0.248	0.210	0.210	
	P (W/kg)	133.9	120.5	102.6	89.28	75.89	75.89	
(B)	A (mW)	0.80	0.725	0.625	0.575	0.525	0.475	59.35%
	q (mC/cm²)	20.00	18.12	15.62	14.37	13.12	11.87	
	Cs (F/g)	17.85	16.18	13.95	12.83	11.71	10.60	
	E (Wh/kg)	0.396	0.359	0.310	0.285	0.260	0.235	
	P (W/kg)	142.8	129.4	111.6	102.6	93.75	84.82	

3.5.5 Electrochemical impedance Spectroscopy

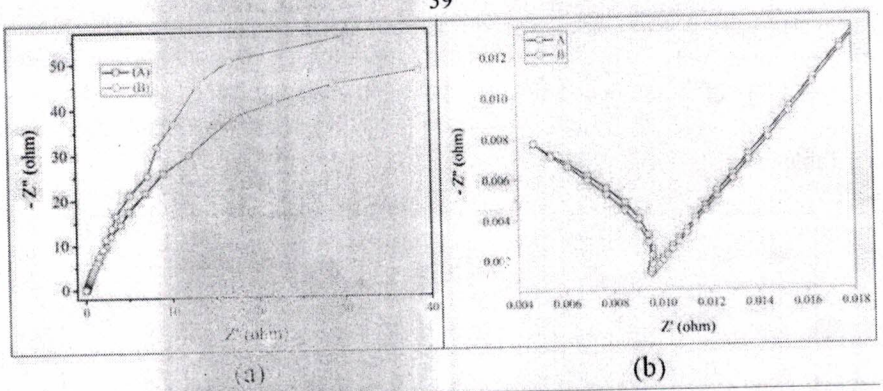

Fig 7 (a) EIS curves of electrodes (A) & (B); (b) at high and medium frequency, enlarged EIS curves of (A) & (B) electrodes.

AC impedance spectroscopy was used to measure the resistance associated with electrolyte solution between reference electrode and working electrode, active electrode material and interface of electrode/electrolyte. The EIS study was carried out with ac voltage of amplitude 5mV, in the frequency range of 0.01Hz to 1.5MHz. The Nyquist plots between the real part of impedance Zý (K&!) and the imaginary part of impedance Z3 (K&!) are presented in Fig. 7. The locus of the curve/line of the plot of real and imaginary part of impedance is composed of a half semicircle at high frequency (> 10^4Hz), a straight line at middle frequency (10^4 Hz to 1Hz) and again a semicircle at low frequency (< 1Hz). In high frequency region, the internal resistance is due to electrolyte solution, active material particles and contact between particles of active material having lower value shows conductivity. The diameter of the semicircle represents the charge transfer resistance of NCs electrode, but with electrodeposition time it increases slightly. At the middle region of frequency, a sloppy straight line yielded a small phase angle for NCs electrodes. Non-conducting electrode generally yields a phase angle of 45°, while diffusion control in a semi-infinite pore yields a phase angle of 22.5° [36], hence NC electrodes confirmed better diffusion of Na^+/OH^- ions in middle frequency region [36, 37].

Conclusion

Electrochemical deposition synthesis of amorphous PANI-Ni(OH)2 electrodes was carried out at room temperature. For synthesizing NC electrodes, a two-step electrodeposition method was applied. The SC values, estimated from the CV areas, of NC electrodes (A) and (B) measured at 10 mV/s scan rate in 1.0M NaOH were 20.08 F/g & 33.48 F/g respectively. The variation of q, Cs, E and P demonstrated a same nature of decrease in values of electrodes (A) and (B) with retention of 56.6% and 59.35% respectively, indicating an improvement in the cyclic stability of NC electrodes with time of electrodeposition. The retention in q, Cs and E is same and is 66.6% & 37.3% respectively

for electrodes (A) and (B). NC electrodes confirmed better diffusion of $Na^+/OH>$ ions in middle frequency region.

References

1) P. Simon, Y. Gogotsi, Nat. Mater. 7 (2008) 845.

2) Y. Zhai, Y. Dou, D. Zhao, P. F. Fulvio, R. T. Mayes, S. Dai, Adv. Mater., 22 (2011) 4828.

3) A. S. Aric, P. Bruce, B. Scrosati, J.M. Tarascon, W. van Schalkwijk, Nat. Mater., 4 (2005)366.

4) C. Liu, F. Li, L. P. Ma, H. M. Cheng, Adv. Mater. 22 (2010) E28.

5) S. W. Lee, B. M. Gallant, H. R. Byon, P. T. Hammond, Y. Shao-Horn, Energy Environ. Sci., 4 (2011) 1972.

6) H. Zhang, G. Cao, Y. Yang, Energy Environ. Sci., 2 (2009) 932.

7) D. N. Futaba, K. Hata, T. Yamada, T. Hiraoka, Y. Hayamizu, Y. Kakudate, O. Tanaike, H. Hatori, M. Yumura, S. Iijima, Nat. Mater., 5 (2006) 987.

8) J. Liu, G. Cao, Z. Yang, D. Wang, D. Dubois, X. Zhou, G. L. Graff, L. R. Pederson, J.G. Zhang, ChemSusChem, 1 (2008) 676.

9) D. W. Wang, F. Li, J. P. Zhao, W.C. Ren, Z. G. Chen, J. Tan, Z. S. Wu, I. Gentle, G. Q. Lu, H. M. Cheng, ACS Nano, 3 (2009) 1745.

10) H. W. Park, T. Kim, J. Huh, M. Kang, J. E. Lee, H. Yoon, ACS Nano, 6 (2012) 7624.

11) W. S. Huang, B. D. Humphrey, A. J. MacDiarmid, J. Chem. SOC., Faraday Trans., 1, 1986, 2385.

12) G. Wang, L. Zhang, J. Zhang, Chem. Soc. Rev., 41 (2012) 797.

13) T. Liu, L. Finn, M. Yu, H. Wang, T. Zhai, X. Lu, Y. Tong, Y. Li, Nano Lett., 14, 2014, 2522.

14) H. Xu, J. Zhang, Y. Chen, H. Lu J. Zhuang, RSC Adv., 4, 2014, 5547.

15) Y. Tian, S. Cong, W. Su, H. Chen, Q. Li, F. Geng, Z. Zhao, Nano Lett., 14, 2014, 2150.

16) H. Fan, H. Wang, N. Zhao, X. Zhanga , J. Xu, J. Mater. Chem., 22, 2012, 2774.

17) H. Wang, Q. Hao, X. Yang, L. Lu, X. Wang, Nanoscale, 2, 2010, 2164.

18) H. Jiang, T. Zhao, C. Li, J. Ma, J. Mater. Chem., 21, 2011, 3818.

19) J. Zhang, L. B. Kong, J. J. Cai, H. Li, C. Luo, L. Kang, Microp. Mesop. Mater., 2010, 132, 154.

20) F. Shi, L. Li, X. L. Wang, C. D. Gu and J. P. Tu, RSC Adv., 2014, 4, 41910.

21) H. Chen , L. Hu , Y. Yan , R. Che , M. Chen , L. Wu, Adv. Energy Mater., 2013, 3, 1636.

22) W. Zhou, X. Cao, Z. Zeng, W. Shi, Y. Zhu, Q. Yan, H. Liu, J. Wang, H. Zhang, Energy Environ. Sci., 2013, 6, 2216.

23) S. Yang, X. Wu, C. Chen, H. Dong, W. Hub, X. Wang, Chem. Commun., 2012, 48, 2773.
24) L. Jiang, R. Zou, W. Li, J. Sun, X. Hu, Y. Xue, G. He, J. Hu, J. Mater. Chem. A, 2013, 1, 478.
25) C. Tang, X. Yin, H. Gong, ACS Appl. Mater. Interfaces, 2013, 5, 10574.
26) K. Wang, J. Huang, Z. Wei, J. Phys. Chem. C, 2010, 114, 8062.
27) D. A. Corrigan, R. M. Bendert, J. Electrochem. Soc., 1989, 136, 723.
28) C. C. Streinz, A. P. Hartman, S. Motupally, J. W. Weidner, J. Electrochem. Soc., 1995, 142, 1084.
29) D. Zhao, W. Zhou, H. Li* Chem. Mater., 2007, 19, 3882.
30) M. S. Wu, Y. A. Huang, C. H. Yang, J. Electrochem. Soc., 155, 2008, A798.
31) H. Wang, H. S. Casalongue, Y. Liang, H. Dai, J. Am. Chem. Soc., 2010, 132, 7472.
32) J. Ji, L. L. Zhang, H. Ji, Y. Li, X. Zhao, X. Bai, X. Fan, F. Zhang, R. S. Ruoff, ACS Nano, 7, 6237, 2013.
33) D. A. Corrigan, R. M. Bendert, J. Electrochem. Soc., 1989, 136, 723.
34) F. S. Cai, G. Y. Zhang, J. Chen, X. L. Gou, H. K. Liu, S. X. Dou, Angew. Chem., Int. Ed., 2004, 43, 4212.
35) S. K. Meher, P. Justin, G. R. Rao , ACS Appl. Mater. Interfaces, 3 (2011) 2063.
36) D.D. Macdonald, Electrochim. Acta, 51 (2006) 1376.
B. E. Conway, Electrochemical Supercapacitors Scientific: Fundamentals and Technological Applications, 1st ed.; Kluwer Academic/ Plenum Press, New York, 1999, p521.